American Journal of Climate Change, 2022, 11, 133-154
https://www.scirp.org/journal/ajcc
ISSN Online: 2167-9509
ISSN Print: 2167-9495

Distribution and Oceanic Dynamic Mechism of Precipitation Induced by Typhoon Lekima

Linxu Huang[1], Ruixue Cao[1*], Shuwen Zhang[2]

[1]College of Ocean and Meteorology, Guangdong Ocean University, Zhanjiang, China
[2]Institute of Marine Science, Shantou University, Shantou, China
Email: huanglinxu1@stu.gdou.edu.cn, *caorx@gdou.edu.cn, zhangsw@stu.edu.cn

How to cite this paper: Huang, L. X., Cao, R. X., & Zhang, S. W. (2022). Distribution and Oceanic Dynamic Mechism of Precipitation Induced by Typhoon Lekima. *American Journal of Climate Change, 11,* 133-154.
https://doi.org/10.4236/ajcc.2022.112007

Received: March 22, 2022
Accepted: June 20, 2022
Published: June 23, 2022

Abstract

Air-sea interaction usually affects the distribution of precipitation during typhoon period, but whether typhoon precipitation distribution is affected by ocean eddies is still unclear. In this study, based on a multi-source satellite database, reanalysis data and in-situ data were used to study the precipitation characteristics of Typhoon Lekima (2019) as well as its physical causes. The results showed that the precipitation of Lekima presents an asymmetric structure, exhibiting heavier precipitation on the left side of the typhoon path before 7 August, and with the typhoon strengthened, precipitation was evenly distributed around the typhoon center. The typhoon cloud system, characteristics of the typhoon, and ocean factors could be responsible for the asymmetric structure of precipitation during the typhoon period. The change in the typhoon cloud system during the typhoon influenced the distribution of precipitation. And there have been some oceanic processes that influenced the distribution of precipitation. Anticyclonic eddies and thick mixing level depths (MLDs) play important roles in typhoon precipitation. The anticyclonic eddies with thick MLD exist to reduce the mixing of the upper ocean to maintain the SST. Therefore, the SST and air-sea exchange can be sustained to influence typhoon precipitation. This study provides a new understanding of the impact of ocean processes on typhoon precipitation distribution.

Keywords

Typhoon Lekima, Ekman Pumping, Ocean Mixing, Mesoscale Eddies, Precipitation

1. Introduction

A tropical cyclone (TC) is a cyclone generated in the tropical ocean basins, it is accompanied by strong wind, precipitation and other weather phenomena. The precipitation of TC comes from eyewalls, spiral rainbands and interaction between typhoon circulation and other weather systems (Chen et al., 2010). The favourable condition for precipitation is that there is sufficient water vapour with a strong vertical wind shear (VWS). The environmental VWS affects rainfall asymmetries in typhoons (Marks, 1984; Merrill, 1988; Black et al., 2002; Chan et al., 2004; Gao et al., 2009; Yu et al., 2010; Yue et al., 2015; Chen et al., 2006; Cecil, 2007; Yu et al., 2017). The greater the relative humidity in the lower troposphere, the more abundant the water vapour content, and the convergence of the lower troposphere, the divergence of the upper troposphere with the vertical upward movement of the troposphere, the stronger the convective activity of the troposphere, and the greater the latent heat released by the upward movement leads to more typhoon precipitation. The spatial distribution of typhoon precipitation is enhanced along the left side of its path (Fu et al., 2020). Precipitation can regulate ocean salinity and temperature, also affect the heat budget between the ocean and the atmosphere. Precipitation directly dilutes the sea water, resulting in a decrease in salinity on the sea surface. In addition, precipitation affects sea water temperature by influencing dynamic processes.

The air-sea exchange process can influence the precipitation and it is also influenced by the temperature. Strong winds of TC can cause strong mixing in the upper ocean, including entrainment and vertical mixing, resulting in a strong uplift of the thermocline (Stramma et al., 1986; Price, 1981). The entrainment effect mixes a large amount of cold subsurface seawater with warm mixed layer seawater, which reduces the temperature of the upper ocean. The entrainment effect on the right side of the typhoon track is more intense than that on the left side because the mixing layer current velocity and the entrainment intensity on the right side of the typhoon path is larger than that on the left side, resulting in a stronger sea surface cooling on the right side of typhoon path (Price, 1981; Chu et al., 2000; Liu et al., 2009). The wind speed on the right side of the typhoon track rotates clockwise, in line with the direction of the Ekman Current in the Northern Hemisphere, causing resonance effects in the ocean (Stramma et al., 1986; Price, 1981). Additionally, the left side of the typhoon track is deflected by a cyclone, and the rotation direction is forced to reverse with the Coriolis force in the Northern Hemisphere so that the energy transfer on the right side of the typhoon track is greater than that on the left side, and the response intensity on the right side is greater than that on the left side (Chang & Anthes, 1979). At the same time, the decrease in sea surface temperature will have an obvious negative feedback effect on typhoon intensity, weakening or even closing the energy supply of the ocean to the typhoon (Timmermann et al., 2005).

Mesoscale eddies are widely distributed in the ocean, and in the Northern Hemisphere, the central temperature of a cyclonic eddy is lower than that of the surrounding sea surface, also known as a cold eddy. In contrast, anticyclonic eddies have higher central temperatures than the surroundings. Statistical results evidence that the strength, size, propagation speed of mesoscale oceanic eddies can be significantly influenced by tropical cyclones, especially for cold core eddies. These eddies can modulate the air-sea enthalpy exchange, and thereby have a potentially important role in influencing local atmosphere after the passage of tropical cyclones (Ma et al., 2021). The relatively unstable thermodynamic structure of the cold eddy enhances the dynamic response of the upper ocean when the typhoon passes, making cold water easier to disturb and lift and causing surface cooling (Stramma et al., 1986). In addition, a cold eddy also intensifies and enlarges after typhoon crossed. The existence of a warm eddy is similar to an insulator. When a typhoon passes through a warm eddy, it can effectively suppress the decrease in sea surface temperature caused by the typhoon itself, and the intensity of the typhoon may be enhanced (Lin et al., 2005). A positive sea surface temperature anomaly (SSTA) with a warm eddy may induce an increase in the sea surface wind (SSW) speed, cloud properties and rainfall, and a negative SSTA with a cold eddy may decrease these parameters (Frenger et al., 2013).

Previous studies have clarified that typhoon precipitation has asymmetry along its path (Lv et al., 2009; Yu et al., 2015), and the upper ocean response is also asymmetric (Price, 1981; Chu et al., 2000; Liu et al., 2009; Chang & Anthes, 1979). The ocean provides energy for typhoon development by air-sea exchange. However, whether typhoon precipitation distribution is affected by the ocean is still unclear. Thus, Super Typhoon Lekima (3-14 August 2019) provided an opportunity to study such an event.

2. Materials and Methods

2.1. Data

The typhoon data were obtained from the China Meteorological Administration (CMA) tropical cyclone database (http://tcdata.typhoon.org.cn/) (Ying et al., 2014; Lu et al., 2021), including the location of the typhoon centre, maximum sustained wind speed, minimum central pressure and tropical cyclone (TC) intensity with a time resolution of 6 h. Super typhoon Lekima originated in the western Pacific. Lekima information is shown in **Figure 1**, moving along the northwest direction. Lekima is a Super Typhoon with rapidly intensification. It was made landfall in East of China and resulted in significant damage across several provinces. It is a typical example of typhoon development and the precipitation characteristics. Lekima first formed as a tropical storm (TS) at 17.5˚N, 130.3˚E at 12:00 on 4 August 2019 (UTC, as follows). Then, Lekima moved slowly northwestward and upgraded to a strong tropical storm (STS) at 18:00 on 5 August 2019. At 18:00 on 6 August 2019, Lekima reached the typhoon (TY) level. Approximately 18 hours later, Lekima upgraded to a strong typhoon (STY) and moved fast (>4 m/s). At 18:00 on 7 August 2019, Lekima strengthened to a super typhoon (Super TY) and was maintained until 00:00 on 9 August. It weakened to an STY at 6:00 on 9 August and maintained its intensity at 12:00 on 9 August. Three hours later, it strengthened to a Super TY again, and finally, it landed in Zhejiang Province, China.

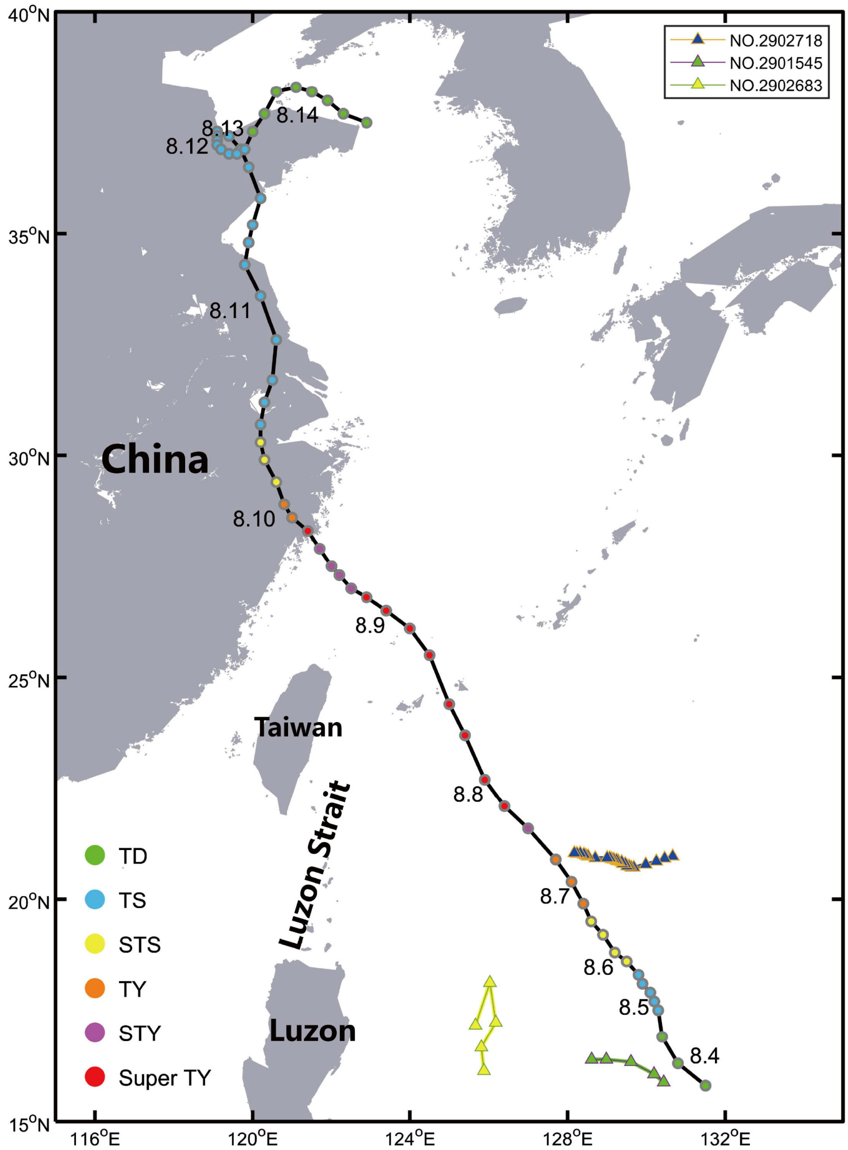

Figure 1. Typhoon Lekima tracks and intensity changes with the Argo track. The coloured dots indicate the centre of typhoon. The black line denotes typhoon path. The yellow triangles denote float NO. 2902683, the green triangles denote float NO. 2901545, and the blue triangles denote float NO. 2902718.

The buoy data was obtained from the China Array for Real_time Geo-strophic Oceanography (Argo, http://www.argodatamgt.org/) from buoys NO. 2901545, NO. 2902683, and NO. 2902718 and included seawater pressure (dbar), seawater temperature (˚C) and seawater salinity (psu). Argo NO. 2901545 and NO. 2902683 with a temporal resolution of 10 days. Argo NO. 2902718 with a resolution of 1 day on August 5 to 14 during Lekima process. The locations of these buoys and their dates are shown in **Figure 1**.

The temperature of blackbody brightness (TBB) data from Himawari-8 satellite observations of the Japan Meteorological Agency (JMA) were obtained with a 11.2 μm tunnel and a pixel resolution of approximately 0.02˚ × 0.02˚.

The satellite of the Tropical Rainfall Measuring Mission (TRMM) from the National Aeronautics and Space Administration (NASA) provided precipitation data with high spatial (0.25˚) and temporal (3 h) resolution.

Copernicus Marine Environment Monitoring Service (CMEMS) provided daily sea level anomaly (SLA) and geostrophic velocity data with a spatial resolution of 0.25˚ × 0.25˚. And the weekly mixing level depths (MLDs) data with spatial (0.25˚) resolution.

The reanalysis data of sea surface temperature (SST), sea surface latent heat flux (SLHF) and near-surface 10 m wind are from the European Centre for Medium-Range Weather Forecast (ECMWF) ERA-5 database (https://cds.climate.copernicus.eu/) with a spatial resolution of 0.25˚ × 0.25˚ and a temporal resolution of 6 h. The daily mean data were averaged from four times (00:00, 06:00, 12:00, 18:00).

2.2. Methods

2.2.1. Empirical Orthogonal Function (EOF)

Empirical orthogonal function (EOF) analysis was performed by extracting the main data features in the matrix. These methods have been widely used in atmospheric and marine scientific research. Generally, the feature vector corresponds to the spatial sample, and the principal component corresponds to the time change. We refer to the spatial patterns as EOFs, and the time series as principal components (PCs).

2.2.2. Ekman Pumping

Typhoon wind stress ($\vec{\tau}$) causes the ocean Ekman pumping effect, which is the main mechanism of the upper ocean response and can be calculated by:

$$\left(\tau_x, \tau_y\right) = \rho_a C_D \left(u\sqrt{u^2+v^2}, v\sqrt{u^2+v^2}\right) \tag{1}$$

where τ_x and τ_y are the components of $\vec{\tau}$ in the meridional and zonal directions, respectively; u and v are the ocean surface 10 m wind velocities in the meridional and zonal directions, respectively; $\rho_a = 1.26\,\text{kg}/\text{m}^3$ is the air density; and $C_D = \left(0.73 + 0.069(u,v)\right) \times 0.001$ is the wind stress drag coefficient.

The Ekman pumping velocity (EPV) can be used to represent the ocean Ekman pumping strength, and it can be calculated by (Price, 1981):

$$\text{EPV} = \frac{1}{\rho_0} \nabla \times \left(\frac{\vec{\tau}}{f}\right) \tag{2}$$

where $\rho_0 = 1024\,\text{kg}/\text{m}^3$ is the sea water density and $f = 2\omega \sin\theta$ is the Coriolis parameter.

3. Results

3.1. Characteristics of Typhoon Precipitation Distribution

For Lekima, the spatial distribution of precipitation also shows obvious asymmetry, and in **Figures 2(a)-(e)**, the precipitation shows a left bias, which is consistent

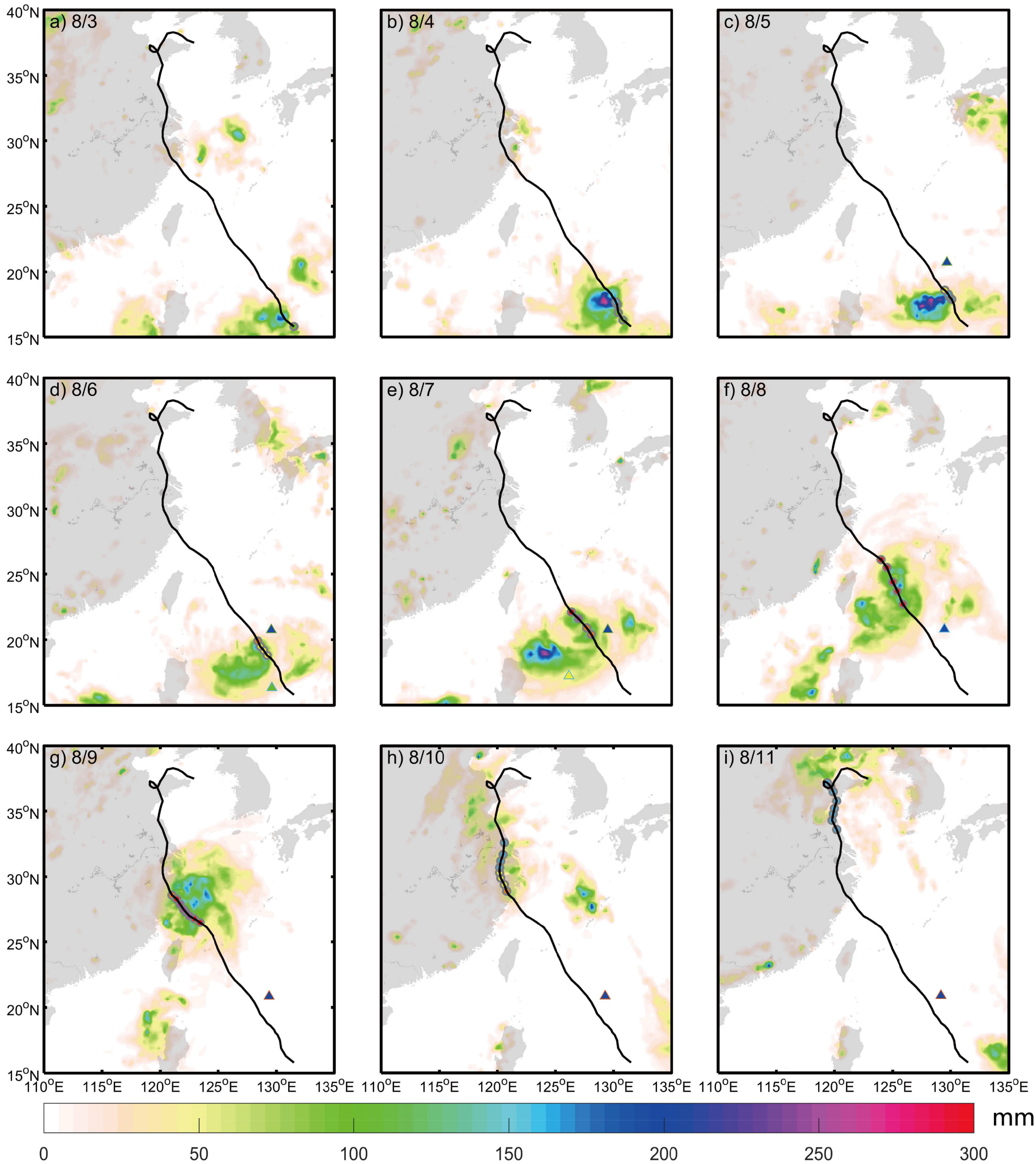

Figure 2. The daily precipitation (shading) variation of Lekima. The coloured dots indicate the centre of typhoon. The black line denotes typhoon path. The yellow triangle denotes float NO. 2902683, the blue triangle denotes float NO. 2901545, and the blue triangle denotes float NO. 2902718.

with the results of a previous study (Marks, 1984; Merrill, 1988). However, as shown in Figure 2(a), there was some rainfall on the right side of the Lekima path. In Figure 2(b), the maximum rainfall was near the typhoon centre. After 7 August, precipitation began to appear on the right side of the path (Figures

2(f)-(h)). The asymmetry of typhoon precipitation was shown to decrease with increasing TC intensity (Xu et al., 2014). The intensity of typhoons is proportional to the average precipitation rate. The greater the intensity is, the greater the average precipitation rate and the closer the maximum precipitation position is to the typhoon centre (Lonfat et al., 2004). When Lekima made landfall, the rainfall decreased with a scattered distribution, but there was some rainfall in the southwest of the typhoon (**Figure 2(h)**). On the other hand, it is noteworthy that the precipitation on the left side of Luzon Island on 8 to 9 August (**Figures 2(f)-(g)**) cannot be ignored.

3.2. Distribution of SLA, SST and MLD

Figure 3 shows the evolution of the SLA and the geostrophic current fields during Lekima. The research area shows that the SLA was dominated by positive anomalies. We defined the positive SLA (anticyclonic eddy) feature (closed contours, SLA > 6 cm) and the negative SLA (closed contours, SLA < −6 cm) feature (Sun et al., 2014). There were two anticyclonic eddies on the right side of the Lekima path and one anticyclonic eddy on the left side. On August 4, there was an obvious cyclonic eddy on the path of Lekima (**Figure 3(b)**), and after the Lekima pass, the cyclonic eddy strength decreased by 7.19 cm. Another cyclonic eddy east of Taiwan strengthened slightly. The SLA from 11 August to 7 August decreased by 0.98 cm.

As shown in **Figure 4**, the region of the west Pacific had a high SST (>30˚C) on 3 August, and after Lekima passed the ocean, it caused the ocean SST to decrease. It is obvious that the SST cooling on the right side of the Lekima path was greater than that on the left side (**Figure 4**). The maximum cooling centre was located in the cyclone strengthening region along the typhoon track. On 11 August, the cooling centre temperature was 2.83˚C lower than that on 2 August (the day before Lekima originated). At 00:00 on 8 August, Lekima, with a rapid translation speed (6.12 m/s), moved northwestward and made the maximum cooling occur on the right side of the typhoon centre. According to previous studies, for rapidly moving (>6 m/s) typhoons, the maximum cooling occurs on the right side of the typhoon path (approximately 70 km), and for slowly moving (<4 m/s) typhoons, the maximum cooling occurs near or on its path (Stramma et al., 1986; Price, 1981).

The mixing level depth (MLD) can be used to show ocean mixing, and when it deepens, ocean mixing is also strong. In general, the shallower the MLD is, the stronger the resulting sea surface cooling (Bender & Ginis, 2000; Lin et al., 2008; Lin et al., 2009). **Figure 5(a)** & **Figure 5(b)** shows the ocean MLD distribution before Lekima; the MLD was relatively weak (<50 m), but it was stronger on the right side than on the left side. Therefore, the right side of the Lekima path was colder than the left, and the air-sea heat exchange on the left side of Lekima would also be stronger than that on the right side, yielding left bias in the precipitation. During the Lekima passing period, precipitation increased obviously on

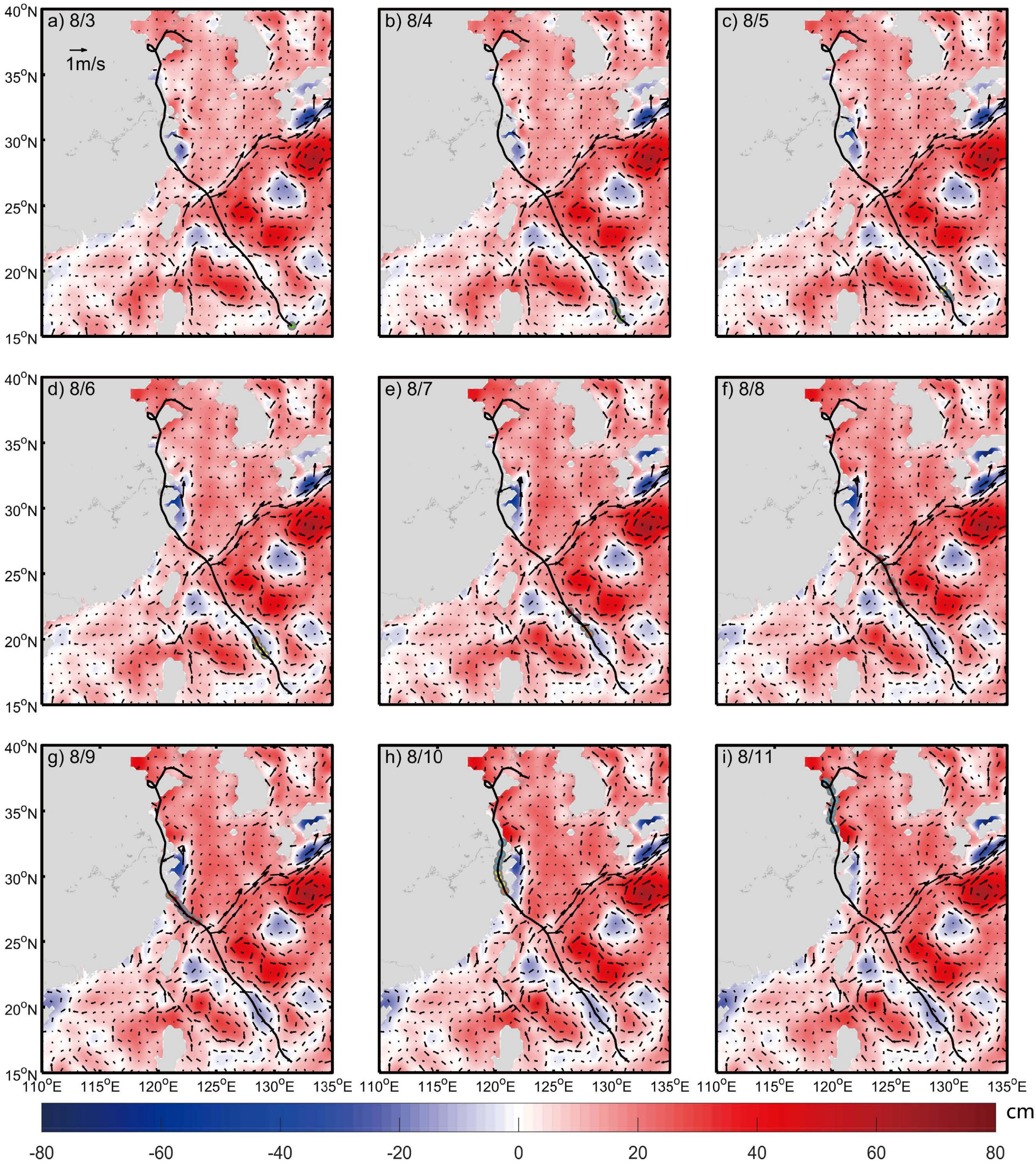

Figure 3. The difference in sea level anomalies (shading) and geostrophic currents (arrows). The black line denotes typhoon path.

the left side of the Lekima path (**Figure 5(c)** & **Figure 5(d)**). A few days after Lekima passed, the MLD continued to deepen, and the maximum deepening of the MLD area originated in southwestern Lekima (**Figure 5(e)** & **Figure 5(f)**). Generally, the MLD was deeper on the right side of the typhoon than on the other side because of the ocean response, which was stronger on the right side of

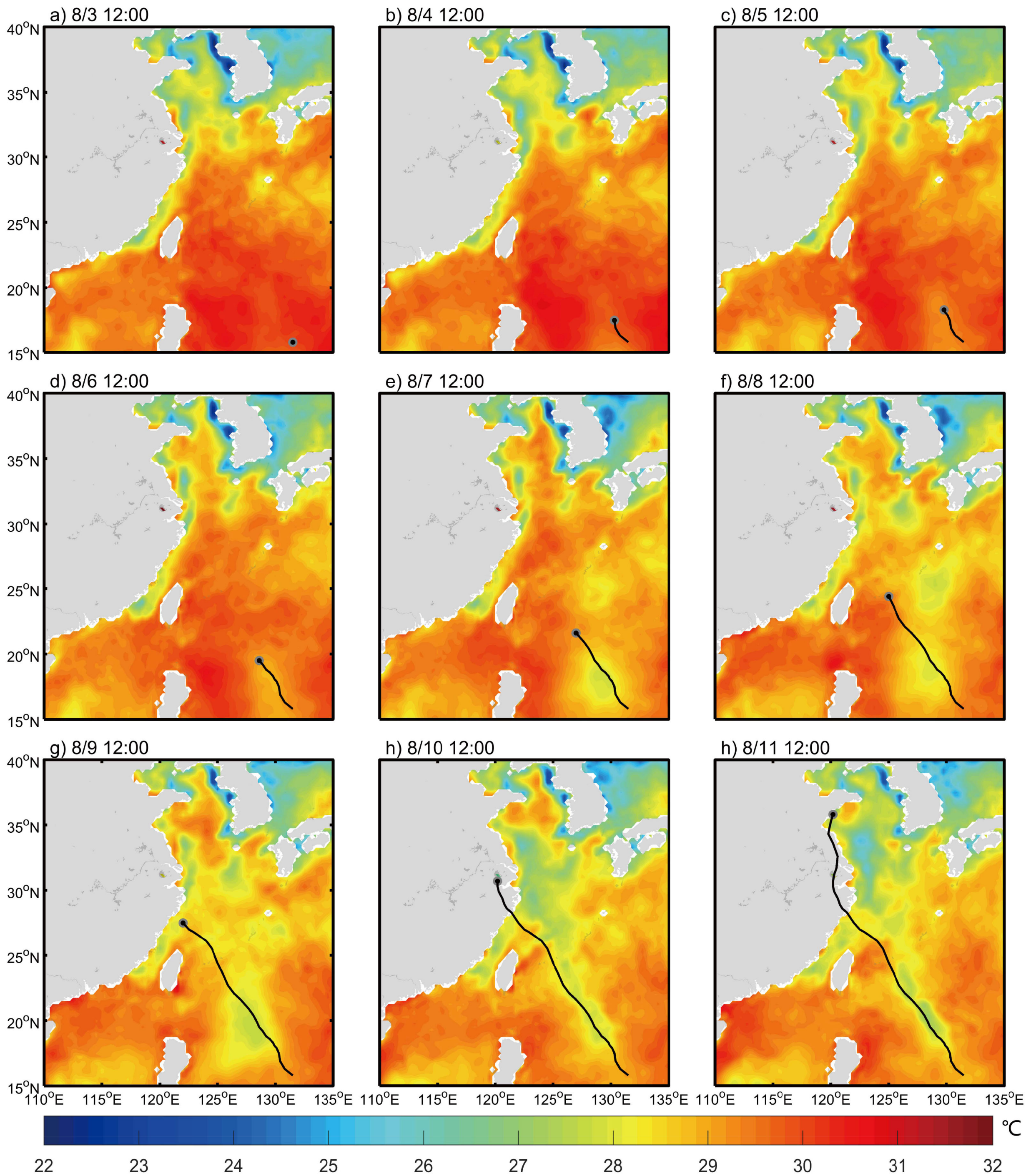

Figure 4. The distribution of SST (shading). The black line denotes typhoon path.

the typhoon path than on the left (Price, 1981). However, for Lekima, the MLD on the left side of the typhoon path was obviously deeper (Figure 5).

4. Discussion

4.1. Characteristics of Typhoon Cloud Systems

Typhoon cloud systems have asymmetric spiral structures, and their internal

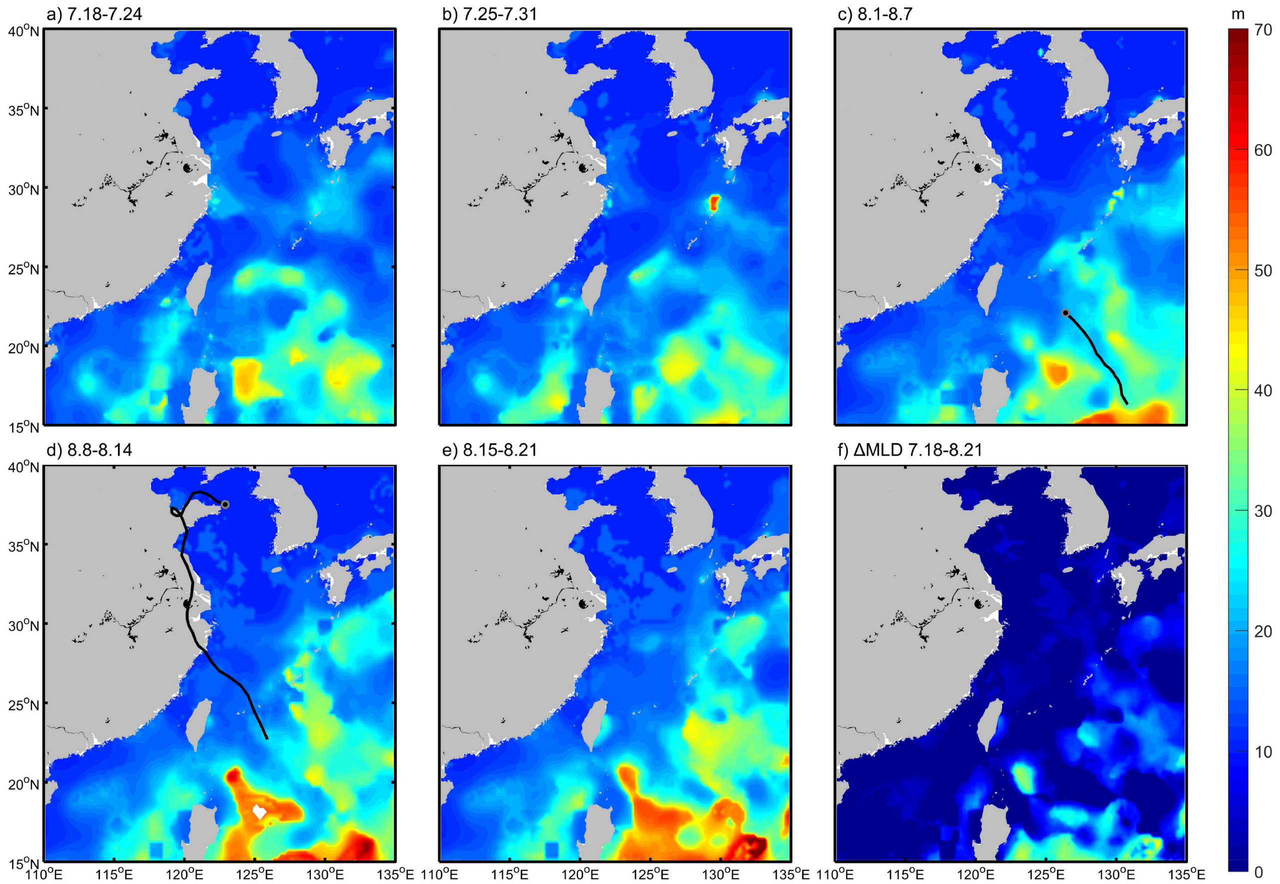

Figure 5. Variation in MLD (shading). The black line denotes typhoon path.

cloud microphysical processes are closely related to typhoon rainfall intensity and area. The TBB reflects the height of the cloud top; the lower the value is, the stronger the vertical movement. With a stronger vertical upward movement, there is more precipitation. Before 12:00 on 7 August, the northeast side of the cloud system lacked the development of cloud clusters, and the convection was concentrated to the west and southwest. The TBB is relatively low on the left side of the typhoon centre, and the precipitation is asymmetric, which is more than the left side of the typhoon path. At 12:00 on 7 August, the cloud system of Lekima showed an obvious vortex structure with a clear typhoon eye, a complete circulation structure in the centre of the typhoon, and strong typhoon convection continued until the typhoon landed. During this period, the typhoon precipitation area expanded (Figure 2). At 12:00 on 9 August, a spiral cloud band on the southwest side of Lekima began to dissipate (Figure 6(f)). Until 12:00 on 10 August, the southwest spiral rainband dissipated as sporadic convective clouds, and the core convective area of the typhoon shrank gradually, with a spiral rainband on the east (Figure 6(g)). After that, the peripheral circulation structure of Lekima was loose, and the cyclonic circulation also weakened. Therefore, the change in typhoon cloud structure affects the distribution of typhoon precipitation.

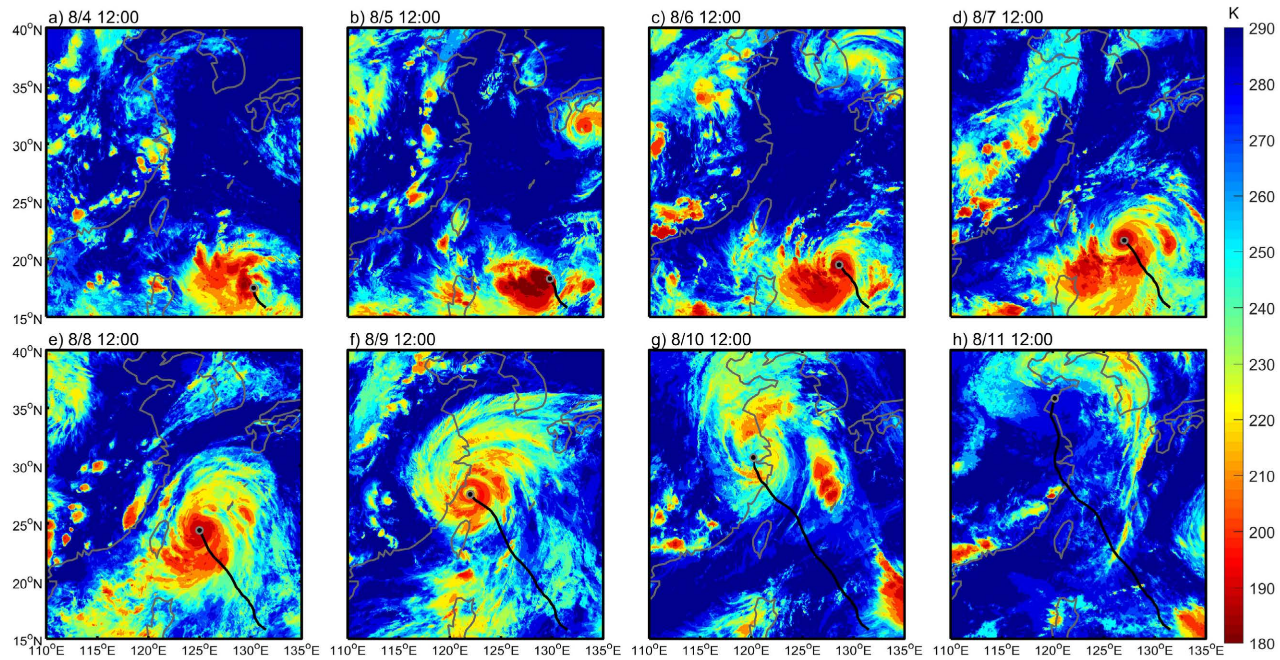

Figure 6. The cloud characteristic of typhoon Lekima. The black line denotes typhoon path.

4.2. Atmospheric Circulation

The mid-high latitudes are shown as "two troughs and one ridge", and the ridge line is located between the two troughs (Figure 7(a) & Figure 7(b)). The subtropical high pressure is mainly located in the sea, with strong intensity and obvious ridge line. The west extension point is mainly located over Shandong Province. The trough originally located in Shanxi Province moved eastward, and the trough in Northeast China weakened and disappeared. Affected by the trough, the subtropical high pressure moved eastward. As shown in Figure 7(c) & Figure 7(d), it developed into "one trough and one ridge". At the same time, Lekima was located in the southwest side of subtropical high pressure, and strengthen gradually. At 12:00 on August 7 (Figure 7(e)), the low pressure system along the north of the subtropical high pressure affects the development of the trough ridge. To August 8 (Figure 7(f)), there was a multi-shortwave trough activity in the middle latitudes. The westward movement of the subtropical high pressure was blocked, and the westward extension point was close to 126˚E. At that time, Typhoon Krosa was located on the east side of Lekima which had a distance about 1500 km. After that, Lekima moves northwest under the guidance of southeast airflow south of the subtropical high pressure. At the same time, the tropical disturbance in the low latitude area is extremely active. The south side of Lekima was connected with the southwest jet, and the water vapor also the energy were continuously input. The south of Lekima developed vigorously, which the intensity also increased rapidly. After the typhoon landed (Figure 7(h)), the westerly trough moved eastward and approached, and Lekima moved northward mainly. The northern side of the typhoon was affected by weak cold air, and the convection was enhanced. Then, Lekima moved southward to

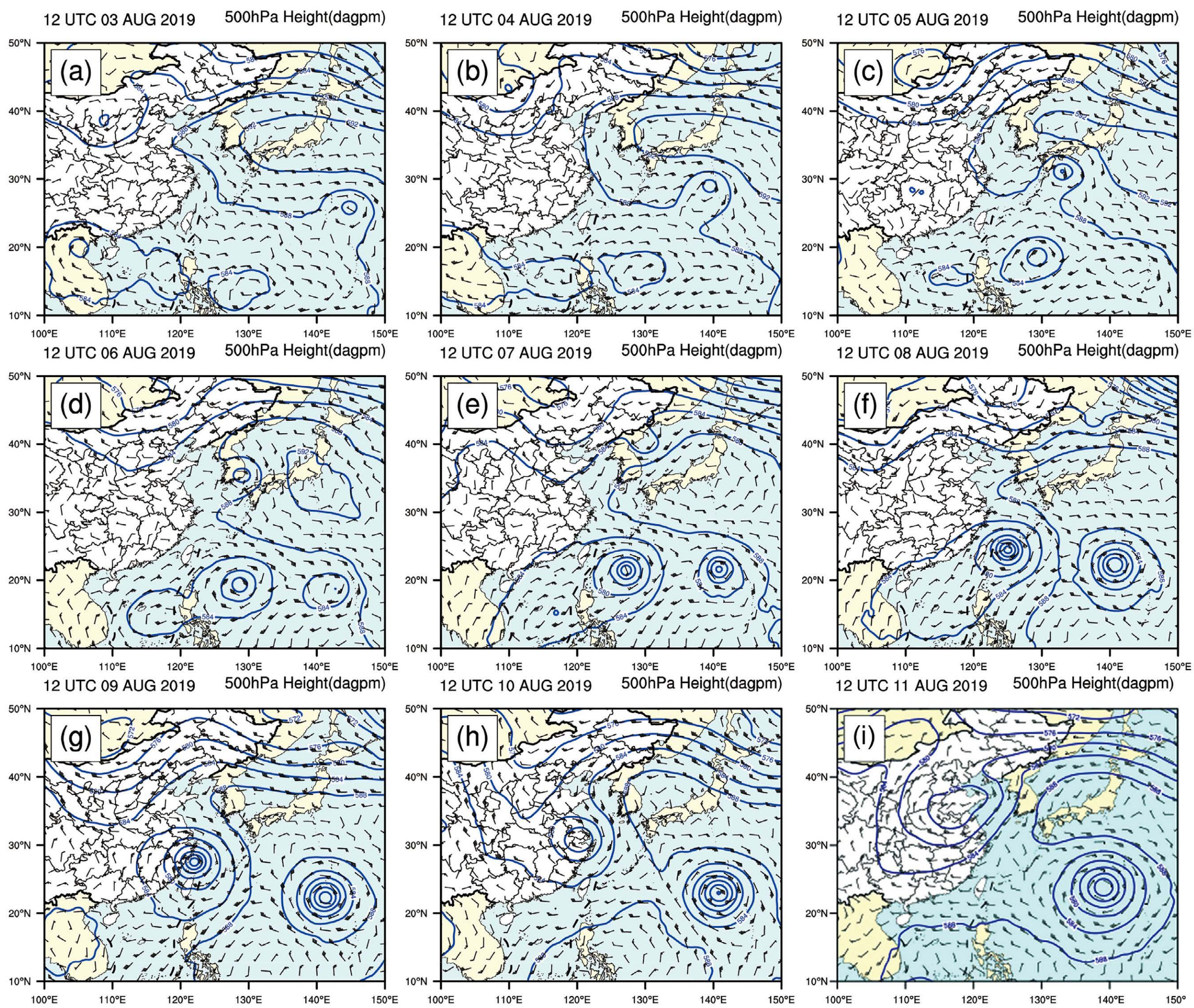

Figure 7. 500 hPa geopotential height field (the blue lines) and wind (wind-direction shaft).

obtain the westerly trough. At 12:00 on 11 August, the trough developed and strengthened. A low pressure system appeared over North China, and the intensity reached 576 hPa, and Typhoon Krosa also strengthened.

4.3. Difference of SLA, SST and MLD

SST can be affected by mesoscale eddies and ocean mixing. The spatial and temporal modes of SLA are shown in Figure 8. The first mode contribution rate was 49.83%, and the second mode contribution rate was 29.59%. The second temporal mode of SLA was dominated by Lekima and reached a maximum on 15 August. Before 7 August, the temporal mode of EOF-2 was negative, and from 8 to 23 August, the temporal mode of EOF-2 became positive. The spatial mode of EOF-2 suggested that the SLA variation was caused by Lekima when the temporal mode of EOF-2 changed from negative to positive. On the other hand, the spatial mode and temporal mode of EOF-1 clearly showed the mesoscale

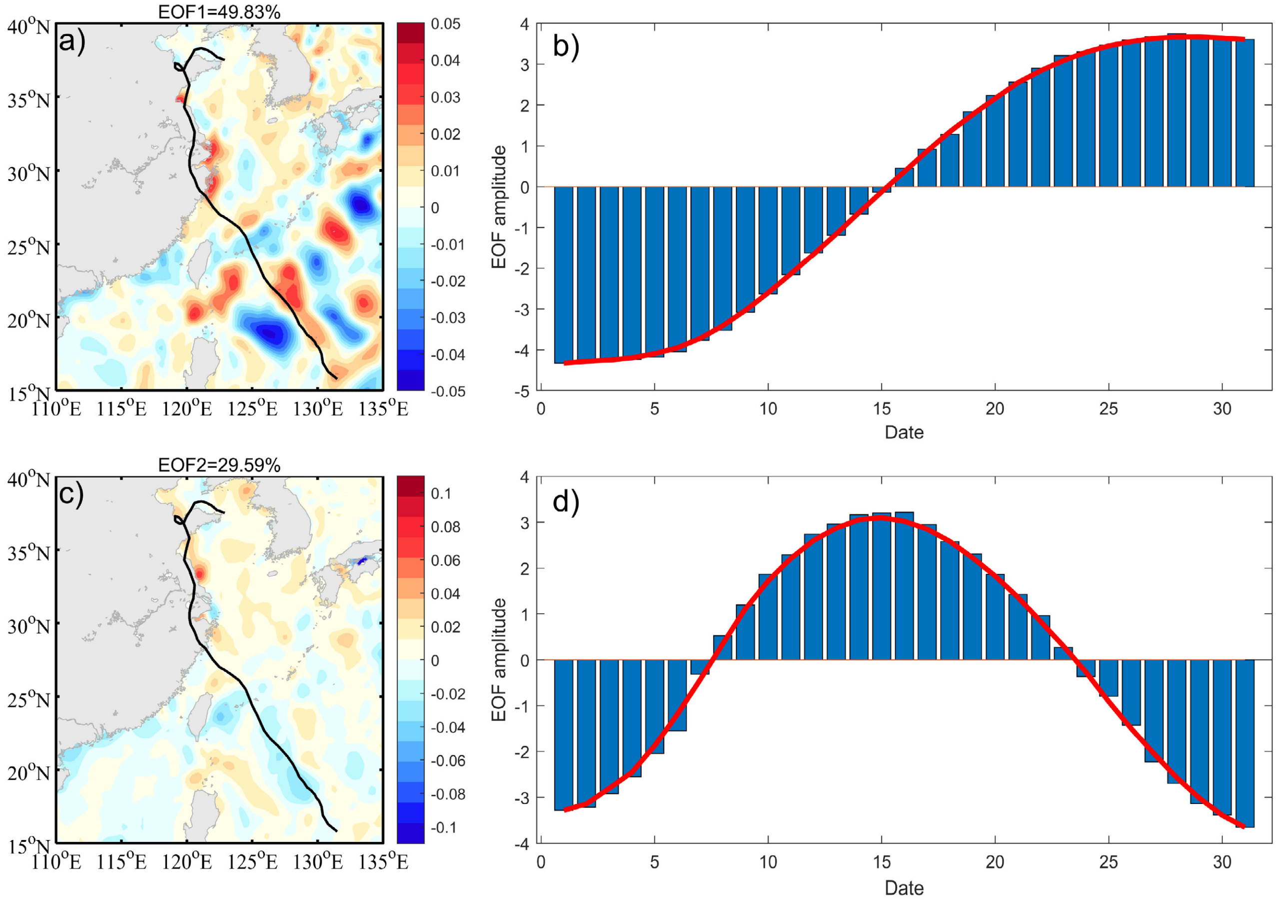

Figure 8. The spatial and temporal characteristics of SLA. The first spacial (a) and temporal (b) mode. The second spacial (c) and temporal (d) mode.

eddy distribution on both sides of the Lekima path. Before 15 August, the anticyclonic eddy on the left side of the Lekima path was strong. Therefore, the anticyclonic eddy area has a high SST and low cooling caused by Lekima.

The spatial and temporal modes of SST are shown in Figure 9. The first mode contribution rate was 49.12%, and the second mode contribution rate was 23.74%. The second temporal mode of SST was dominated by Lekima and reached peaks on August 10. Before 6 August, the temporal mode was negative. However, the daily oscillation was reversed on 7 August. From 7 August, the daily oscillation remained positive until 20 August. The spatial mode of SST shows that the distribution of SST is high in the north and low in the south. The spatial mode and temporal mode of EOF-1 clearly showed that the area was warm before 14 August. The spatial mode of EOF-2 suggested that the SST variation was caused by Lekima when the temporal mode of EOF-2 changed from negative to positive.

Ocean mixing leads to cooling of surface seawater and warming of subsurface seawater, which is the heat pump effect of typhoons. After Typhoon Lekima passed, the depth of the mixing layer also significantly increased in depth, the depth of the mixing layer in the ocean was stronger than that in the nearshore

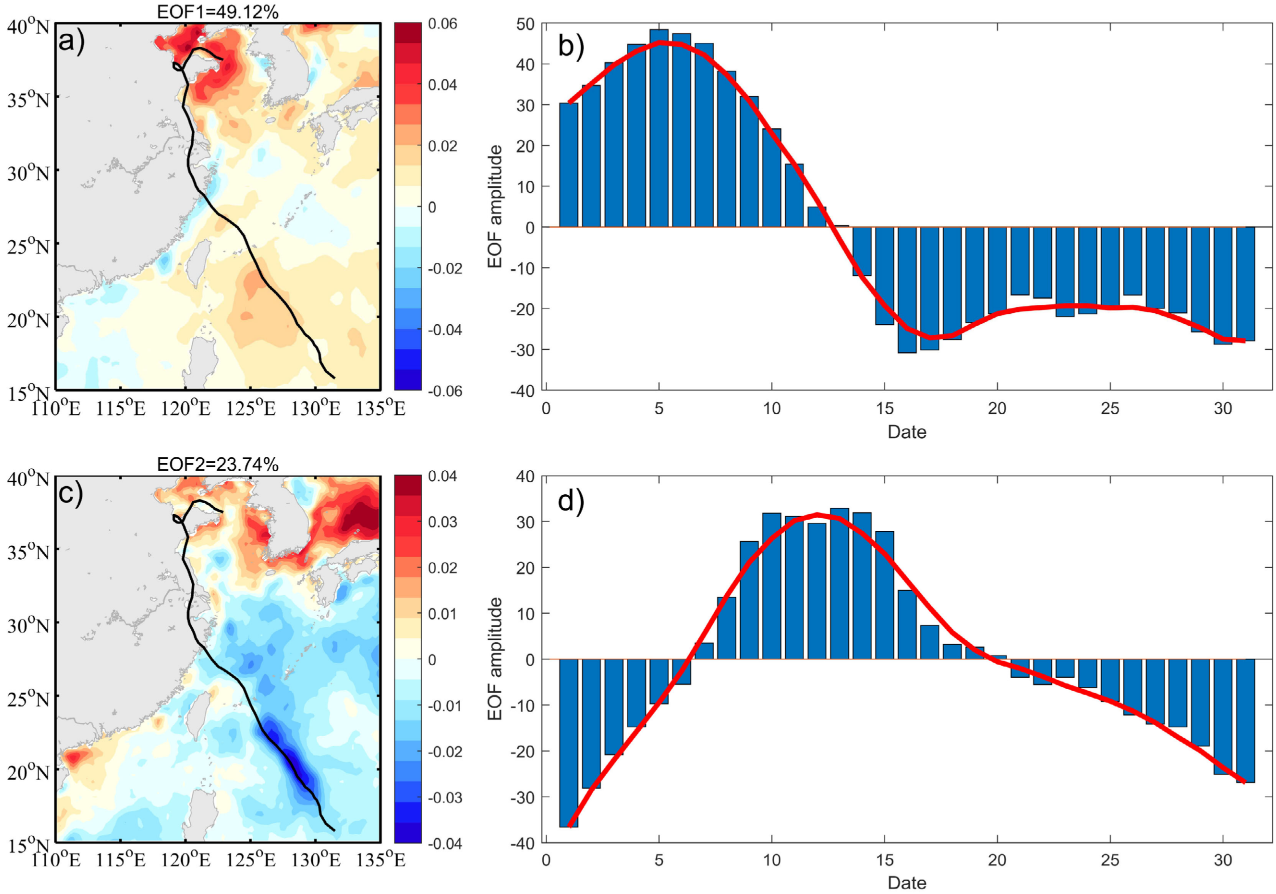

Figure 9. The spatial and temporal characteristics of SST. The first spacial (a) and temporal (b) mode. The second spacial (c) and temporal (d) mode.

ocean, and the depth of the mixing layer on the left side of the typhoon path was deeper than that on the other side. We captured three buoy datasets, ignoring the influence of seawater density, salinity and sea surface anomaly processes, and the depth of the mixed layer was defined as 0.8˚C lower than the 10 m seawater temperature (Kara et al., 2000). The calculation results are shown in **Table 1**.

The temperature of the mixed layer of buoy No. 2901545, located on the left side of the Lekima path, was significantly lower on 6 August than on 27 July (**Figure 10(a)**), and the depth of the mixed layer deepened significantly. By 16 August, the MLD decreased and the salinity of the mixed layer increased (**Figure 10(b)**), but the temperature of the mixed layer hardly changed. The No. 2902683 buoy was located on the left side of Lekima, and the temperature of the mixed layer decreased significantly on August 7 compared with that on July 28. The MLD increased in depth, but increase was small (**Figure 10(c)**), and the salinity of the mixed layer decreased significantly (**Figure 10(d)**). Precipitation may have a great impact on the buoy measuring point. By 17 August, the salinity of the mixed layer rebounded, and the salinity change was stronger than the temperature change. The NO. 2902718 buoy located on the right side of the Lekima path captured the data of each day from 5 August to 14 August. As shown in

Table 1. MLDs of the floats.

Argo	Date	Location	MLD/m
2901545	7.17	16.385˚N, 128.611˚E	37.37
	7.27	16.386˚N, 128.983˚E	34.28
	8.6	16.331˚N, 129.609˚E	65.00
	8.16	16.057˚N.130.193˚E	47.67
	8.26	15.874N, 130.439˚E	76.21
2902683	7.18	17.161˚N, 125.655E	69.28
	7.28	18.12˚N, 126.031˚E	43.93
	8.7	17.226˚N, 126.18˚E	50.66
	8.17	16.662˚N, 125.814˚E	74.83
	8.27	16.131˚N, 125.880˚E	56.31
2902718	7.17	20.971˚N, 130.667˚E	30.38
	7.21	20.924˚N, 130.462˚E	39.47
	7.26	20.858˚N, 130.253˚E	30.36
	7.31	20.789˚N, 129.984˚E	44.74
	8.5	20.721˚N, 129.681˚E	39.41
	8.6	20.746˚N, 129.559˚E	48.80
	8.7	20.752˚N, 129.509˚E	66.56
	8.8	20.800˚N, 129.464˚E	66.25
	8.9	20.843˚N, 129.398˚E	69.70
	8.10	20.863˚N, 129.286˚E	54.28
	8.11	20.901˚N, 129.170˚E	54.22
	8.12	20.911˚N, 129.117˚E	52.64
	8.13	20.931˚N, 129.071˚E	58.31
	8.14	20.935˚N, 129.004˚E	60.33
	8.19	20.932˚N, 128.702˚E	42.21
	8.22	20.971˚N, 128.521˚E	43.35
	8.23	20.988˚N, 128.466˚E	47.43
	8.24	21.014˚N, 128.414˚E	48.82
	8.25	21.038˚N, 128.322˚E	41.56
	8.26	21.045˚N, 128.172˚E	51.91

Table 1, the temperature of the mixed layer decreased significantly on 6 August, and the MLD deepened greatly. Until 14 August, the temperature of the mixed layer was still decreasing (Figure 10(e)), and the depth of the mixed layer was also deepening, which may be related to the influence of the mesoscale eddies generated by Lekima. The salinity of the mixed layer increased on 6 August (Figure 10(f)) and did not change significantly until 14 August.

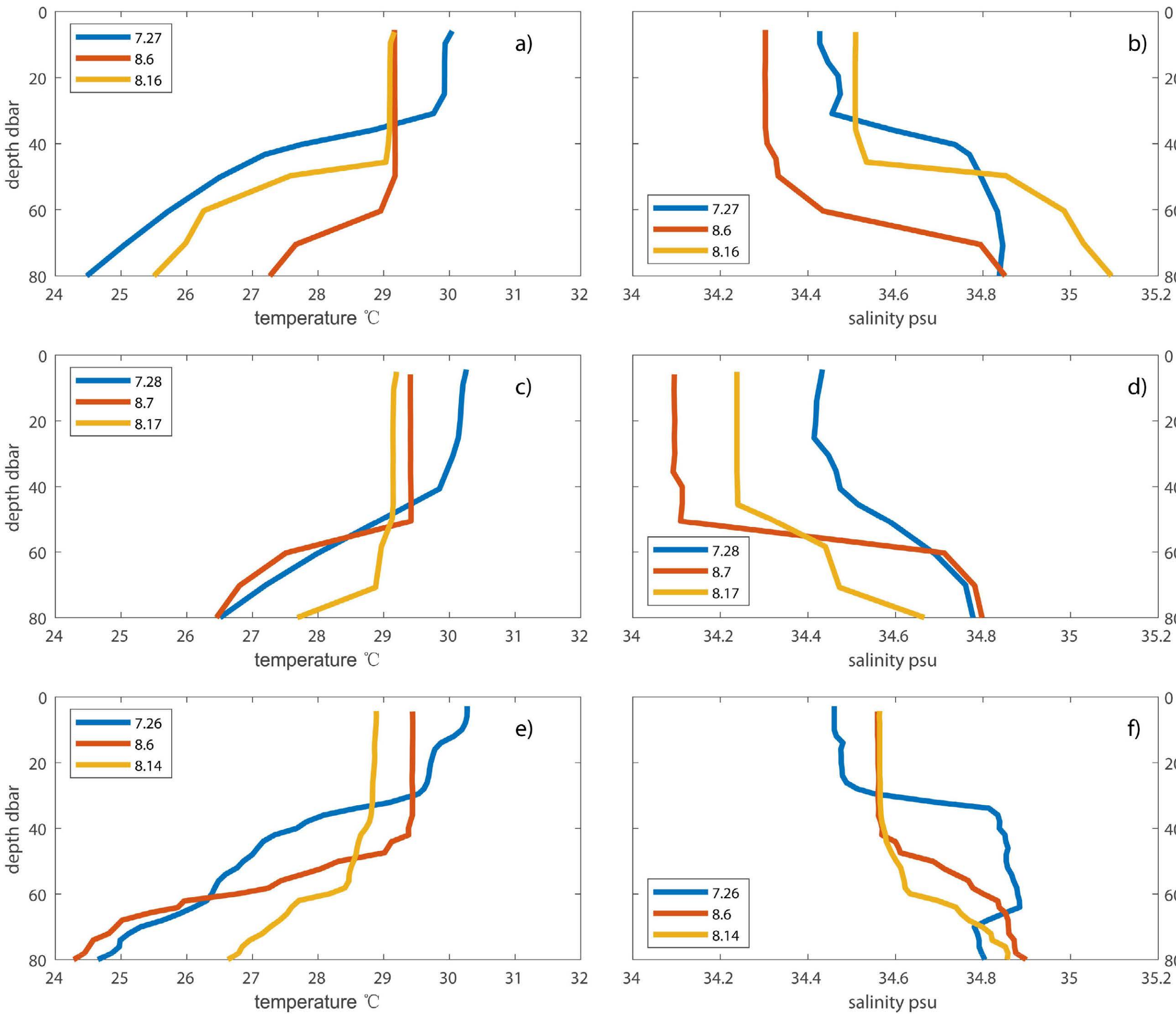

Figure 10. Vertical temperature and salinity distribution of the upper ocean.

It can be seen from satellite remote sensing data and buoy data that the depth deepening of the mixing layer on the left side of the Lekima path is greater than that on the right side, which may be because the anticyclonic eddies on the right side of the typhoon path inhibit the entrainment mixing caused by typhoon wind. Both warm eddies and thick MLDs influence typhoon precipitation under VWS conditions. Since anticyclonic eddies have thick MLDs, the wind of typhoons can hardly mix surface seawater and deep seawater. Thus, the SST of anticyclonic eddy areas has slightly decreased with relatively stronger sea-air exchange. Thus, the anticyclonic eddy area would have more precipitation than the others.

4.4. Ekman Pumping and Variation of SLHF

The cyclone wind field caused strong wind stress by typhoons, which caused Ekman pumping and mixing of the upper ocean (Chiang et al., 2011; Zhang et al., 2016). In general, near the typhoon centre, the positive EPV is upward and upwelling, and the negative EPV is downward and downwelling. The upwelling causes cold water in the deep mixing layer to flow up, resulting in a decrease in sea surface temperature. At the same time, deep sea water with high salinity is brought to the sea surface, which causes the sea surface salinity to increase. The cooling from the upwelling effect of a typhoon is called cold suction. Downwelling could transfer heat from the ocean surface to the ocean interior, increasing the temperature of the ocean interior. At 12:00 on 4 August, it is obvious that the upwelling on the right side of Lekima's path (**Figure 11(b)**). Then, the upwelling occurred around the typhoon centre, and the EPV reached a maximum value on

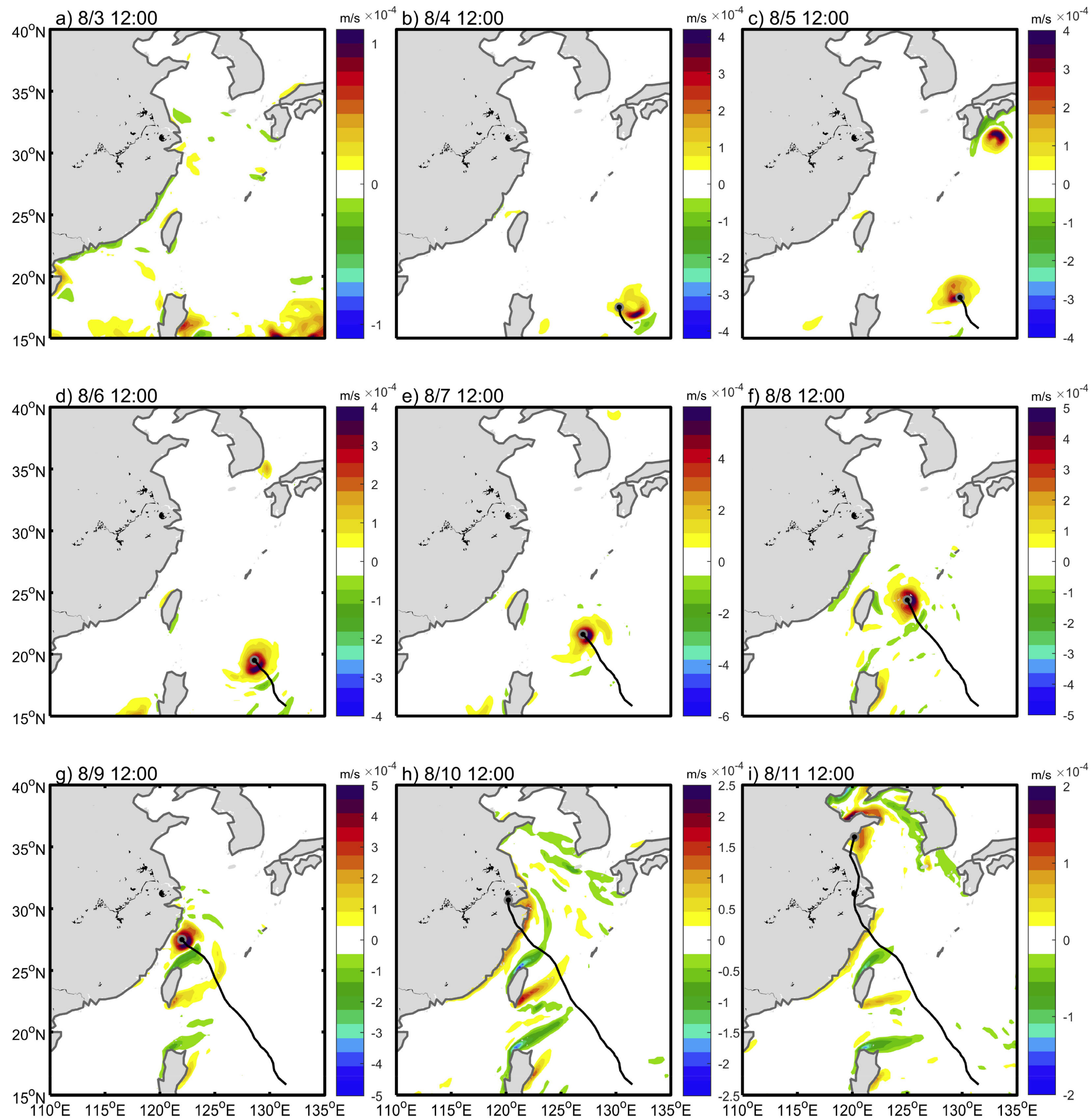

Figure 11. Variation in Ekman pumping velocity (shading). The green line denotes typhoon path.

7 August. After that, the value of EPV began to decrease. Strong Ekman pumping leads to a lower SST and weaker air-sea exchange in the upwelling region, resulting in less precipitation on the right of the Lekima path to the left on 4 August. With the weakening of Ekman pumping on the right side, the anticyclonic eddies on the right side began to inhibit SST cooling, and the air-sea heat exchange was also stronger than that in the other regions, so precipitation began to appear on the right side of the Lekima path.

The air-sea interface enters the atmosphere through the sea surface in the form of latent heat flux and sensible heat flux. The SLHF is related to evaporation

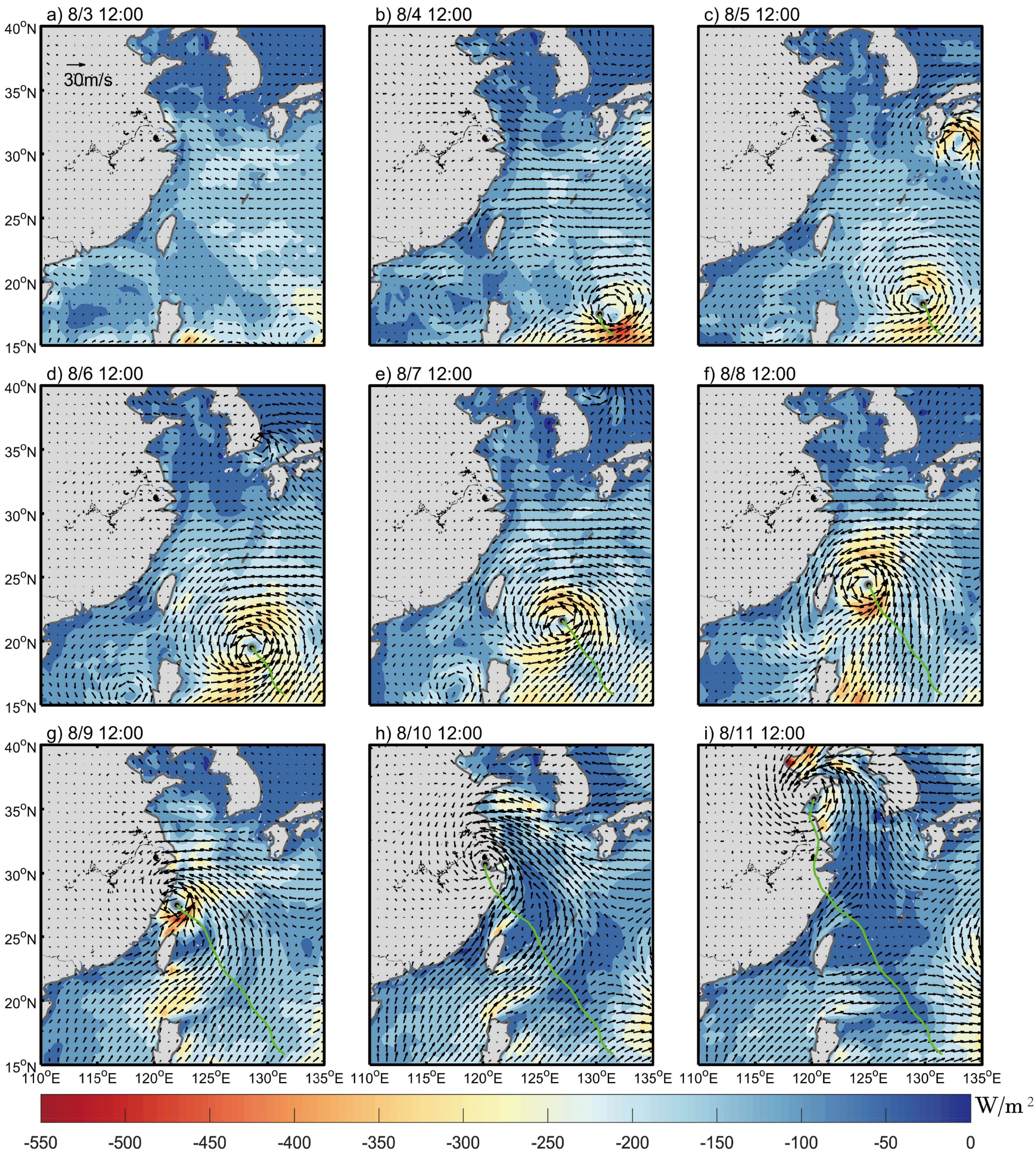

Figure 12. Diurnal variation in SLHF (shading) and 10 m wind (arrows). The green line denotes typhoon path.

which provides sufficient water vapor conditions for typhoon precipitation. The more the SLHF output is, the stronger the water vapor transport is. Also evaporation transmits ocean energy to the atmosphere in the form of latent heat to maintain the occurrence and development of typhoons. Surface moisture convergence from the surrounding atmosphere and the underlying sea surface must provide the moisture for condensation heating. In Figure 12, the SLHF from ocean loss was concentrated near the typhoon centre and was closely related to its cloud structure. Clouds can reduce the ocean absorption of solar shortwave radiation and increase longwave radiation. In the Northern Hemisphere summer, which is strongly affected by the southwest monsoon, the southwesterly wind will carry a large amount of warm and humid airflow, providing favourable conditions for precipitation. In Figure 2, the precipitation area corresponds to the convergence area of southwest wind and the typhoon's perturbation current. The large value area of SLHF reduction has a good corresponding relationship with precipitation and downwelling area, especially the precipitation in the Luzon Strait. When Lekima landfall, the SLHF has decreased but precipitation has increased due to strong vertical upward movement.

5. Conclusion

Based on the multisatellite database, reanalysis data and in-situ Argo float data, we presented here the significant physical cause of typhoon Lekima's precipitation with atmospheric and ocean factors. The precipitation of Typhoon Lekima is spatially asymmetric, and the precipitation on the left side is larger than that on the right side before 7 August, which is related to the warm eddy existing with the thick MLD on the left side of the Lekima path. After 7 August, Lekima began to be affected by the eddies on the right side of the Lekima path, and the MLD change on the right side of Lekima was not stronger than that on the other side. Because warm eddies have thick MLDs, the wind of typhoons cannot mix surface seawater and deep seawater. Because of this, the SST of warm eddy areas also sustained sea-air exchange. Therefore, precipitation began to appear on the right side of the Lekima path. The upwelling may lead to SST cooling, but the downwelling caused by Lekima wind stress is consistent with the spatial distribution of latent heat lost during typhoon transit. We still do not know the mechanism between downwelling and SLHF, which needs further study. We considered whether the factors caused by the typhoon itself, including MSW, central pressure and translation speed, are correlated with typhoon precipitation. In addition, we also calculated the correlation coefficient between SLHF and precipitation. The results show that the SLHF and central pressure had a negative correlation with typhoon precipitation and that the MSW with typhoon precipitation had a positive correlation. The translation speed of typhoons had no correlation with precipitation.

Funding

This work was supported by National Natural Science Foundation of China

92158201, 41876005.

Acknowledgements

We thank 4 anonymous reviewers for their constructive suggestions.

Conflicts of Interest

The authors declare no conflicts of interest regarding the publication of this paper.

References

Bender, M. A., & Ginis, I. (2000). Real-Case Simulations of Hurricane-Ocean Interaction Using a High-Resolution Coupled Model: Effects on Hurricane Intensity. *Monthly Weather Review, 128,* 917-946. https://doi.org/10.1175/1520-0493(2000)128<0917:RCSOHO>2.0.CO;2

Black, M. L., Gamache, J. F., Marks Jr., F. D. et al. (2002). Eastern Pacific Hurricanes Jimena of 1991 and Olivia of 1994: The Effect of Vertical Shear on Structure and Intensity. *Monthly Weather Review, 130,* 2291-2312. https://doi.org/10.1175/1520-0493(2002)130<2291:EPHJOA>2.0.CO;2

Cecil, D. J. (2007). Satellite-Derived Rain Rates in Vertically Sheared Tropical Cyclones. *Geophysical Research Letters, 34.* https://doi.org/10.1029/2006GL027942

Chan, J. C. L., Liu, K. S., Ching, S. E. et al. (2004). Asymmetric Distribution of Convection Associated with Tropical Cyclones Making Landfall along the South China Coast. *Monthly Weather Review, 132,* 2410-2420. https://doi.org/10.1175/1520-0493(2004)132<2410:ADOCAW>2.0.CO;2

Chang, S. W., & Anthes, R. A. (1979).The Mutual Response of the Tropical Cyclone and the Ocean. *Journal of Physical Oceanography, 9,* 128-135. https://doi.org/10.1175/1520-0485(1979)009<0128:TMROTT>2.0.CO;2

Chen, L., Li, Y., & Cheng, Z. (2010). An Overview of Research and Forecasting on Rainfall Associated with Landfalling Tropical Cyclones. *Advances in Atmospheric Sciences, 27,* 967-976. https://doi.org/10.1007/s00376-010-8171-y

Chen, S. S., Knaff, J. A., & Marks Jr., F. D. (2006). Effects of Vertical Wind Shear and Storm Motion on Tropical Cyclone Rainfall Asymmetries Deduced from TRMM. *Monthly Weather Review, 134,* 3190-3208. https://doi.org/10.1175/MWR3245.1

Chiang, T. L., Wu, C. R., & Oey, L. Y. (2011). Typhoon Kai-Tak: An Ocean's Perfect Storm. *Journal of Physical Oceanography, 41,* 221-233. https://doi.org/10.1175/2010JPO4518.1

Chu, P. C., Veneziano, J. M., Fan, C. et al. (2000). Response of the South China Sea to Tropical Cyclone Ernie 1996. *Journal of Geophysical Research: Oceans, 105,* 13991-14009. https://doi.org/10.1029/2000JC900035

Frenger, I., Gruber, N., Knutti, R. et al. (2013). Imprint of Southern Ocean Eddies on Winds, Clouds and Rainfall. *Nature Geoscience, 6,* 608-612. https://doi.org/10.1038/ngeo1863

Fu, D., Zhang, X., Li, X. et al. (2020). Changes in the Hydrodynamic Characteristics of the Upper Layer of the South China Sea during the Period of Super Typhoon Rammasun (2014). *Tellus A: Dynamic Meteorology and Oceanography, 72,* 1-15. https://doi.org/10.1080/16000870.2020.1733745

Gao, S., Meng, Z., Zhang, F. et al. (2009). Observational Analysis of Heavy Rainfall Mechanisms Associated with Severe Tropical Storm Bilis (2006) after Its Landfall. *Monthly Weather Review, 137,* 1881-1897. https://doi.org/10.1175/2008MWR2669.1

Kara, A. B., Rochford, P. A., & Hurlburt, H. E. (2000). An Optimal Definition for Ocean Mixed Layer Depth. *Journal of Geophysical Research: Oceans, 105,* 16803-16821. https://doi.org/10.1029/2000JC900072

Lin, I. I., Pun, I. F., & Wu, C. C. (2009). Upper-Ocean Thermal Structure and the Western North Pacific Category 5 Typhoons. Part II: Dependence on Translation Speed. *Monthly Weather Review, 137,* 3744-3757. https://doi.org/10.1175/2009MWR2713.1

Lin, I. I., Wu, C. C., Emanuel, K. A. et al. (2005). The Interaction of Supertyphoon Maemi (2003) with a Warm Ocean Eddy. *Monthly Weather Review, 133,* 2635-2649. https://doi.org/10.1175/MWR3005.1

Lin, I. I., Wu, C. C., Pun, I. F. et al. (2008). Upper-Ocean Thermal Structure and the Western North Pacific Category 5 Typhoons. Part I: Ocean Features and the Category 5 Typhoons' Intensification. *Monthly Weather Review, 136,* 3288-3306. https://doi.org/10.1175/2008MWR2277.1

Liu, X., Wang, M., & Shi, W. (2009). A Study of a Hurricane Katrina-Induced Phytoplankton Bloom Using Satellite Observations and Model Simulations. *Journal of Geophysical Research: Oceans, 114,* C03023. https://doi.org/10.1029/2008JC004934

Lonfat, M., Marks Jr., F. D., & Chen, S. S. (2004). Precipitation Distribution in Tropical Cyclones Using the Tropical Rainfall Measuring Mission (TRMM) Microwave Imager: A Global Perspective. *Monthly Weather Review, 132,* 1645-1660. https://doi.org/10.1175/1520-0493(2004)132<1645:PDITCU>2.0.CO;2

Lu, X., Yu, H., Ying, M. et al. (2021). Western North Pacific Tropical Cyclone Database Created by the China Meteorological Administration. *Advances in Atmospheric Sciences, 38,* 690-699. https://doi.org/10.1007/s00376-020-0211-7

Lv, M., Zou, L., Yao, M. et al. (2009). Analysis of Asymmetrical Structure of Precipitation in Typhoon Aeres. *Journal of Tropical Meteorology,* No. 1, 22-28.

Ma, Z., Zhang, Z., Fei, J. et al. (2021). Imprints of Tropical Cyclones on Structural Characteristics of Mesoscale Oceanic Eddies over the Western North Pacific. *Geophysical Research Letters, 48,* e2021GL092601. https://doi.org/10.1029/2021GL092601

Marks Jr., F. D. (1984). Evolution and Structure of Precipitation in Hurricane Allen. *Monthly Weather Review, 113,* 909-930. https://doi.org/10.1175/1520-0493(1985)113<0909:EOTSOP>2.0.CO;2

Merrill, R. T. (1988). Environmental Influences on Hurricane Intensification. *Journal of Atmospheric Sciences, 45,* 1678-1687. https://doi.org/10.1175/1520-0469(1988)045<1678:EIOHI>2.0.CO;2

Price, J. F. (1981). Upper Ocean Response to a Hurricane. *Journal of Physical Oceanography, 11,* 153-175. https://doi.org/10.1175/1520-0485(1981)011<0153:UORTAH>2.0.CO;2

Stramma, L., Cornillon, P., & Price, J. F. (1986). Satellite Observations of Sea Surface Cooling by Hurricanes. *Journal of Geophysical Research: Oceans, 91,* 5031-5035. https://doi.org/10.1029/JC091iC04p05031

Sun, L., Li, Y. X., Yang, Y. J. et al. (2014). Effects of Super Typhoons on Cyclonic Ocean Eddies in the Western North Pacific: A Satellite Data-Based Evaluation between 2000 and 2008. *Journal of Geophysical Research: Oceans, 119,* 5585-5598. https://doi.org/10.1002/2013JC009575

Timmermann, A., An, S. I., Krebs, U. et al. (2005). ENSO suppression Due to Weakening of the North Atlantic Thermohaline Circulation. *Journal of Climate, 18,* 3122-3139.

https://doi.org/10.1175/JCLI3495.1

Xu, W., Jiang, H., & Kang, X. (2014). Rainfall Asymmetries of Tropical Cyclones Prior to, during, and after Making Landfall in South China and Southeast United States. *Atmospheric Research, 139,* 18-26. https://doi.org/10.1016/j.atmosres.2013.12.015

Ying, M., Zhang, W., Yu, H. et al. (2014). An Overview of the China Meteorological Administration Tropical Cyclone Database. *Journal of Atmospheric and Oceanic Technology, 31,* 287-301. https://doi.org/10.1175/JTECH-D-12-00119.1

Yu, J., Tan, Z., & Wang, Y. (2010). Effects of Vertical Wind Shear on Intensity and Rainfall Asymmetries of Strong Tropical Storm Bilis (2006). *Advances in Atmospheric Sciences, 27,* 552-561. https://doi.org/10.1007/s00376-009-9030-6

Yu, Z., Wang, Y., & Xu, H. (2015). Observed Rainfall Asymmetry in Tropical Cyclones Making Landfall over China. *Journal of Applied Meteorology and Climatology, 54,* 117-136. https://doi.org/10.1175/JAMC-D-13-0359.1

Yu, Z., Wang, Y., Xu, H. et al. (2017). On the Relationship between Intensity and Rainfall Distribution in Tropical Cyclones Making Landfall over China. *Journal of Applied Meteorology and Climatology, 56,* 2883-2901. https://doi.org/10.1175/JAMC-D-16-0334.1

Yue, C., Gao, S., Liu, L. et al. (2015). A Diagnostic Study of the Asymmetric Distribution of Rainfall during the Landfall of Typhoon Haitang (2005). *Advances in Atmospheric Sciences, 32,* 1419-1430. https://doi.org/10.1007/s00376-015-4246-0

Zhang, H., Chen, D., Zhou, L. et al. (2016). Upper Ocean Response to Typhoon Kalmaegi (2014). *Journal of Geophysical Research: Oceans, 121,* 6520-6535. https://doi.org/10.1002/2016JC012064